Inorg. Chem. **2005**, *44*, 1472–1481

Structure, Spectroscopic Properties, and Reversible Solid-to-Solid Reactions of Metal Complexes of 5-Nitro-pyrimidin-2-olate

Elisa Barea,[†] M. Angustias Romero,[†] Jorge A. R. Navarro,*[,†] Juan M. Salas,*[,†] Norberto Masciocchi,[‡] Simona Galli,*[,‡] and Angelo Sironi[§]

Departamento de Química Inorgánica, Universidad de Granada, Av. Fuentenueva S/N, 18071 Granada, Spain, Dipartimento di Scienze Chimiche e Ambientali, Università dell'Insubria, Via Valleggio 11, 22100 Como, Italy, and Dipartimento di Chimica Strutturale e Stereochimica Inorganica, Università di Milano and Istituto di Scienze e Tecnologie Molecolari del CNR (ISTM-CNR), Via Venezian 21, 20133 Milano, Italy

Received October 19, 2004

In searching for coordination polymers containing the highly polarized 5-nitro-pyrimidin-2-olate ligand (NP), a number of species containing 3d transition metals have been prepared and characterized, namely $Co(NP)_2(H_2O)_4$, $[Co(NP)_2]_n$, $Ni(NP)_2(H_2O)_4$, $[Ni(NP)_2]_x$, and $[Zn(NP)_2]_n$. Their structures have been determined by X-ray powder diffraction methods. The hydrated compounds contain mononuclear $M(NP)_2(H_2O)_4$ units interconnected by means of a three-dimensional (3D) network of hydrogen bonds. The homoleptic species, at variance from the already known metal(II) pyrimidin-2-olate ones, crystallize as two-dimensional (2D) slabs, where the metal coordination is of the MN_3O kind. The electron-withdrawing nitro group, never bound to the metal ion, is likely to influence the observed stereochemistry through steric and dipolar effects within the crystal lattice. The thermal, spectroscopic, and magnetic properties of these species are presented. The $M(NP)_2(H_2O)_4/[M(NP)_2]_{x,n}$ systems interconvert reversibly upon dehydration/rehydration processes.

Introduction

Recently, metal coordination polymers containing polyaza-heteroaromatic ligands have raised the interest of the synthetic and structural chemists, as well as that of the materials scientists in search of tailored species manifesting specific properties. Indeed, the *exo*-bidentate nature of many of these ligands makes them suitable for engineering materials where the metal ion properties can be finely tuned and cooperatively enhanced by easily functionalizable organic spacers.[1] Selected examples, demonstrating the variety of properties manifested by metal polyazolates, include $[Zn(imidazolate)_2]_n$, a promising low-permittivity material,[2] $[Ag(imidazolate)]_n$, a powerful antimicrobial agent,[3] $[Co(imidazolate)_2]_n$, a molecular magnet,[4] and the Fe^{II}(triazole/triazolate) systems, exhibiting spin crossover.[5]

Noteworthy, the vast majority of the polymeric metal azolates are intractable, often polycrystalline, powders, whose structure can only be retrieved by using X-ray powder diffraction (XRPD) methods.[6] Accordingly, in the past decades, we have developed and extensively employed[7] this technique for the complete characterization of, among others, metal diazolates of various kinds.[8] This technique not only allows the structural characterization of these species, but also opens the way to study extended coordination materials

* Author to whom correspondence should be addressed. E-mail: simona.galli@uninsubria.it.
[†] Universidad de Granada.
[‡] Università dell'Insubria.
[§] Università di Milano and Istituto di Scienze e Tecnologie Molecolari del CNR (ISTM-CNR).

(1) See, e.g.: (a) Janiak, C. *Dalton Trans*. **2003**, 2781. (b) Kitagawa, S.; Kitaura, R.; Noro, S. *Angew. Chem., Int. Ed*. **2004**, *43*, 2334.
(2) Świątjek-Tran, B.; Kołodziej, H. A.; Tran, V. H. *J. Solid State Chem.* **2004**, *177*, 1011.
(3) Nomiya, K.; Tsuda, K.; Sudoh, T.; Oda, M. *J. Inorg. Biochem.* **1997**, *68*, 39.
(4) Sánchez, V.; Storr, A.; Thompson, R. C. *Can. J. Chem.* **2002**, *80*, 133.
(5) Roubeau, O.; Haasnoot, J. G.; Codjovi, E.; Varret, F.; Reedijk, J. *Chem. Mater*. **2002**, *14*, 2559.
(6) *Structure Determination from Powder Diffraction Data*; David, W. I. F., Shankland, K., McCusker, L. B., Baerlocher, Ch. Eds.; Oxford University Press: Oxford, 2002.
(7) Masciocchi, N.; Sironi, A. *C. R. Acad. Sci., Ser. IIc: Chim.* **2005**, in press.
(8) Masciocchi, N.; Galli, S.; Sironi, A. *Comments Inorg. Chem.* **2005**, in press.

10.1021/ic048539b CCC: $30.25
Published on Web 02/03/2005

synthesized through unusual solid-to-solid pathways, as well as their corresponding phase transitions in the solid state.[9]

After having deeply investigated the chemistry of metal pyrazolates[10] and imidazolates,[11] we have recently turned our attention to the deprotonated forms of pyrimidin-2-ol and pyrimidin-4-ol and found that their reaction with first row, divalent transition metal ions (Co^{2+}, Ni^{2+}, Cu^{2+}, and Zn^{2+}) gives rise to two- (2D) and three-dimensional (3D) coordination polymers exhibiting extremely high thermal stability or excellent ion pair recognition and gas/liquid sorption properties.[9,12] Additional interesting properties in these systems include second harmonic generation (SHG)[12a] and spin-canted antiferromagnetism.[9a]

In this report, we have transformed the pyrimidin-2-ol into the corresponding 5-nitro derivative (5-nitro-pyrimidin-2-ol, HNP),[13] with the aim of finely tuning the properties of the polymeric $[M(NP)_2]_n$ type species. Thus, in the following, we present the preparation, reactivity, and the complete spectroscopic, thermal, magnetic, and XRPD structural characterization of novel $[M(NP)_2]_x$ species and of some of their (hydrated) precursors, aiming to understand the coordination chemistry of the NP organic moiety, never used, to our knowledge, as a ligand toward metal ions.

For the sake of clarity, the following naming and numbering scheme will be used throughout the paper:

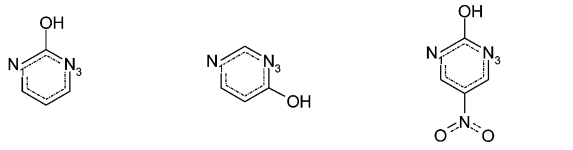

pyrimidin-2-ol (2-Hpymo) pyrimidin-4-ol (4-Hpymo) 5-nitro-pyrimidin-2-ol (HNP)

$Co(NP)_2(H_2O)_4$, $\mathbf{1_{Co}}$ amorphous $[Co(NP)_2]_x$, $\mathbf{2_{Co}}$ crystalline $[Co(NP)_2]_n$, $\mathbf{3_{Co}}$

$Ni(NP)_2(H_2O)_4$, $\mathbf{1_{Ni}}$ amorphous $[Ni(NP)_2]_x$, $\mathbf{2_{Ni}}$

crystalline $[Zn(NP)_2]_n$, $\mathbf{3_{Zn}}$

Results and Discussion

Synthesis and Thermal Behavior of $Co(NP)_2(H_2O)_4$ ($\mathbf{1_{Co}}$), $Ni(NP)_2(H_2O)_4$ ($\mathbf{1_{Ni}}$), Amorphous $[Co(NP)_2]_x$ ($\mathbf{2_{Co}}$), Crystalline $[Co(NP)_2]_n$ ($\mathbf{3_{Co}}$), Amorphous $[Ni(NP)_2]_x$ ($\mathbf{2_{Ni}}$), and $[Zn(NP)_2]_n$ ($\mathbf{3_{Zn}}$). Reaction of 5-nitro-pyrimidin-2-olate (NP) with Co(II) and Ni(II) salts in aqueous solution gives rise to formation of poorly soluble microcrystalline materials of the type $M(NP)_2(H_2O)_4$ ($\mathbf{1_M}$) with the metal ions exhibiting octahedral N_2O_4 chromophores. The water content of $\mathbf{1_M}$ has been confirmed by thermogravimetric and differential scanning calorimetric analyses: the four water molecules are lost in a single-step endothermic process at about 120 and 180 °C for $\mathbf{1_{Co}}$ and $\mathbf{1_{Ni}}$, respectively (ΔH = 198 and 181 kJ mol^{-1}). In both cases, concomitant with dehydration, (i) pronounced color changes, indicative of a modification in the stereochemistry about the metal centers,[14] are observed, and (ii) amorphous compounds of $[M(NP)_2]_x$ formulation are recovered. On cooling these materials at room temperature within 30 min, a crystalline species is recovered in the case of M = Co(II), $\mathbf{3_{Co}}$, whereas for M = Ni(II), the amorphous phase, $\mathbf{2_{Ni}}$, does not evolve into a crystalline one. Amorphous $[M(NP)_2]_x$ may be obtained even by exposing the $\mathbf{1_M}$ species to nonaqueous solvents (ethanol). It is worth noting that the crystalline compound $\mathbf{3_{Co}}$ can also be prepared by either direct reaction of the NP ligand with Co(II) salts in ethanol or by mechanically grinding the parent species $\mathbf{1_{Co}}$. The versatility of the $\mathbf{1_{Co}}-\mathbf{3_{Co}}$ pair is also reflected by the fact that $\mathbf{1_{Co}}$ can be restored by stirring a suspension of $\mathbf{3_{Co}}$ in water for a few minutes. At variance, $\mathbf{2_{Ni}}$ does transform into the parent hydrated species by simply leaving it in humid air for 3 h.

Notably, decomposition of the $\mathbf{3_{Co}}$ and $\mathbf{2_{Ni}}$ species is responsible for large sharp weight loss effects on the TG diagrams taking place at about 460 and 410 °C, respectively. This event (i) confirms the unusual high thermal stability of the analogous metal 2-pyrimidinolates [(T_{dec} = 560 and 550 °C for $[Co(2\text{-pymo})_2]_n$ and $[Ni(2\text{-pymo})_2]_n$, respectively][12a] and (ii) enlightens the similar thermal behavior of the $[M(4\text{-pymo})_2]_n$ compounds (T_{dec} = 470 and 388 °C for M = Co and Ni, respectively),[9a,b] with the Ni(II) species decomposing, in all cases, at a lower temperature (see Table 2). At least in the case of Co(II), it can be pointed out that the trend of T_{dec} for $[Co(2\text{-pymo})_2]_n$, $[Co(4\text{-pymo})_2]_n$, and $[Co(NP)_2]_n$ (560, 470, and 460 °C, respectively) does not follow that of V/Z (235, 225, and 284 $Å^3$, respectively). This may suggest that other effects should be taken into account to explain the lower thermal stability of the NP and 4-pymo systems; actually, electronic effects related to the polarizing nature of the nitro group in the NP ligands, as well as the asymmetry induced by the exocyclic oxygen in the 4-pymo moiety, may facilitate the pyrimidine ring activation during the decomposition process. The two-dimensional nature of the NP and 4-pymo systems, vs the three-dimensional nature of the 2-pymo ones, may also play a non-negligible role.

Reaction of 5-nitro-pyrimidin-2-olate with Zn(II) salts in aqueous solution directly gives the corresponding microcrystalline anhydrous $[Zn(NP)_2]_n$ material, $\mathbf{3_{Zn}}$. Even this material possesses an unusually high thermal stability with a decomposition temperature of 490 °C which, once again, is below that found for the extremely stable $[Zn(2\text{-pymo})_2]_n$ material (T_{dec} = 570 °C)[12a] but much higher than that of $[Zn(4\text{-pymo})_2]_n$ (T_{dec} = 285 °C).[9b]

Spectroscopic Properties of $Co(NP)_2(H_2O)_4$ ($\mathbf{1_{Co}}$), $Ni(NP)_2(H_2O)_4$ ($\mathbf{1_{Ni}}$), $[Co(NP)_2]_n$ ($\mathbf{3_{Co}}$), $[Ni(NP)_2]_x$ ($\mathbf{2_{Ni}}$), and

(9) (a) Masciocchi, N.; Galli, S.; Sironi, A.; Barea, E.; Navarro, J. A. R.; Salas, J. M.; Tabares, L. C. *Chem. Mater.* **2003**, *15*, 2153. (b) Barea, E.; Navarro, J. A. R.; Salas, J. M.; Masciocchi, N.; Galli, S.; Sironi, A. *Inorg. Chem.* **2004**, *43*, 473. (c) Barea, E.; Navarro, J. A. R.; Salas, J. M.; Masciocchi, N.; Galli, S.; Sironi, A. *Polyhedron* **2003**, *22*, 3051.

(10) Masciocchi, N.; Ardizzoia, G. A.; Brenna, S.; LaMonica, G.; Maspero, A.; Galli, S.; Sironi, A. *Inorg. Chem.* **2002**, *41*, 6080 and references therein.

(11) Masciocchi, N.; Castelli, F.; Forster, P. M.; Tafoya, M. M.; Cheetham, A. K. *Inorg. Chem.* **2003**, *42*, 6147 and references therein.

(12) (a) Masciocchi, N.; Ardizzoia, G. A.; La Monica, G.; Maspero, A.; Sironi, A. *Eur. J. Inorg. Chem.* **2000**, 2507. (b) Tabares, L. C.; Navarro, J. A. R.; Salas, J. M. *J. Am. Chem. Soc.* **2001**, *123*, 383. (c) Barea, E.; Navarro, J. A. R.; Salas, J. M.; Masciocchi, N.; Galli, S.; Sironi, A. *J. Am. Chem. Soc.* **2004**, *126*, 3014.

(13) Wempen, I.; Blank, H. U.; Fox, J. J. *J. Heterocycl. Chem.* **1969**, *6*, 593.

(14) Beavais, L. G.; Shores, M. P.; Long, J. R. *J. Am. Chem. Soc.* **2000**, *122*, 2763.

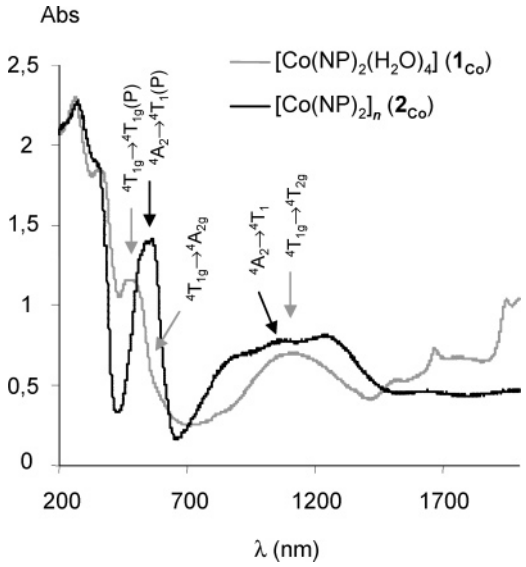

Figure 1. Electronic spectra of $Co(NP)_2(H_2O)_4$ ($\mathbf{1_{Co}}$) and $[Co(NP)_2]_n$ ($\mathbf{3_{Co}}$).

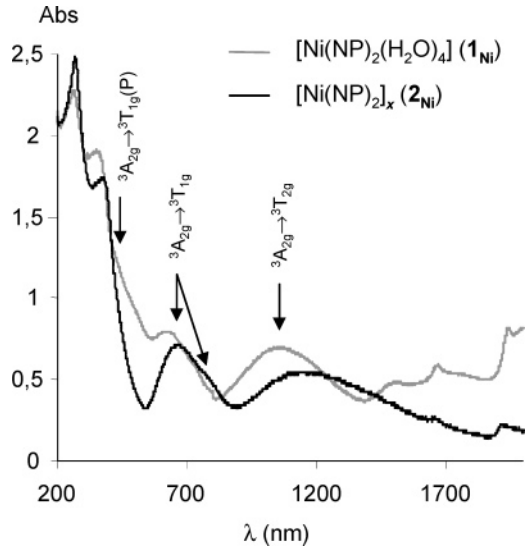

Figure 2. Electronic spectra of $Ni(NP)_2(H_2O)_4$ ($\mathbf{1_{Ni}}$) and $[Ni(NP)_2]_x$ ($\mathbf{2_{Ni}}$).

$[Zn(NP)_2]_n$ ($\mathbf{3_{Zn}}$). IR spectra are indicative of both the nature of the materials and the changes taking place in the samples. For all the species, a very intense band is detectable at about 1335 cm^{-1} because of the presence of the nitro group (1342, 1336, 1328, 1333, and 1330 cm^{-1} for $\mathbf{1_{Co}}$, $\mathbf{1_{Ni}}$, $\mathbf{3_{Co}}$, $\mathbf{2_{Ni}}$, and $\mathbf{3_{Zn}}$, respectively). For the $\mathbf{1_{Co}}$ and $\mathbf{1_{Ni}}$ compounds, the ν(CO) band appears at a lower wavelength than expected (1610 and 1604 cm^{-1}, respectively), indicating, in the presence of *N*-monodentate ligands, a weakening of the C═O bond because of noncovalent interactions involving the exocyclic oxygens (hydrogen bonds, as confirmed by X-ray diffraction). With respect to the ν(CO), $\mathbf{3_{Co}}$ and $\mathbf{3_{Zn}}$ show two different bands, centered at 1664 and 1604 cm^{-1} for the former, and at 1654 and 1611 cm^{-1} for the latter, which suggest two distinct coordination modes for the NP moiety (see below); those centered at 1664 and 1654 cm^{-1} are typical of a *N*,*N*′-*exo*-bidentate coordination mode, while those at 1604 and 1611 cm^{-1} indicate a weakening of the C═O bond, as in the case of a *N*,*O*-*exo*-bidentate coordination fashion. In the case of $\mathbf{2_{Ni}}$, the position of the ν(CO) band slightly shifts to a lower frequency (1597 cm^{-1}) with respect to the parent hydrated species. This may be attributed to the fact that the exocyclic O_3 oxygen, no longer involved in hydrogen bond interactions, should actively participate in the coordination of the metal centers, with the NP ligands probably acting in a μ-η^2-η^1-[(*N*,*O*),*N*′]-tridentate bridging mode.[12a]

The electronic spectra of the Co(II) species $\mathbf{1_{Co}}$ and $\mathbf{3_{Co}}$ (see Figure 1) are indicative of a change in the coordination environment at the metal center upon dehydration, in agreement with the observed different colors of the two compounds. Indeed, while the former is pale pink, typical of an octahedral CoN_2O_4 stereochemistry, $\mathbf{3_{Co}}$ is deep purple, which agrees with a tetrahedral environment about cobalt when surrounded by azaaromatic ligands.[4,12a,15] As shown on the electronic spectra, such a rearrangement implies a deep change in the shape of the electronic spectra, with higher intensity bands typical of tetrahedral chromophores. In the spectrum of $\mathbf{1_{Co}}$, the absorption bands corresponding to the $^4T_{1g} \rightarrow {}^4T_{2g}$ (ν_1) and $^4T_{1g} \rightarrow {}^4T_{1g}(P)$ (ν_3) electronic transitions can be clearly assigned, while the $^4T_{1g} \rightarrow {}^4A_{2g}$ one (ν_2), very weak, appears just as a shoulder. At variance, in the spectrum of $\mathbf{3_{Co}}$, while the absorption bands corresponding to the $^4A_2 \rightarrow {}^4T_1$ (ν_2) and $^4A_2 \rightarrow {}^4T_1(P)$ (ν_3) electronic transitions are clearly observed, the $^4T_{1g} \rightarrow {}^4T_{2g}$ (ν_1) one, occurring in the NIR region, is not detectable. It is worth noting that the $^4A_2 \rightarrow {}^4T_1$ (ν_2) and $^4A_2 \rightarrow {}^4T_1(P)$ (ν_3) transitions, appearing as multiple bands, allow an unequivocal distinction between tetrahedral and octahedral Co(II) stereochemistries.[16] The electronic spectra of $\mathbf{1_{Ni}}$ and $\mathbf{2_{Ni}}$ (see Figure 2) are typical of Ni(II) compounds in octahedral environments. In both, while the bands corresponding to the $^3A_{2g} \rightarrow {}^3T_{2g}$ (ν_1) and $^3A_{2g} \rightarrow {}^3T_{1g}$ (ν_2) electronic transitions are clearly visible, the $^3A_{2g} \rightarrow {}^3T_{2g}$ (ν_3) one is detectable as a modest shoulder quite near to the charge-transfer band in $\mathbf{1_{Ni}}$ but is imperceptible in $\mathbf{2_{Ni}}$. For this reason, the position of this band in $\mathbf{2_{Ni}}$ was estimated by the Dou's method.[17] In both cases, the asymmetry of the ν_2 band is due to a spin−orbit coupling mechanism. In $\mathbf{2_{Ni}}$, this band also appears as a doublet. This fact can be explained, taking into account that the ^1E_g state lies so close to $^3T_{1g}$ that extensive mixing takes place, leading to observation of a doubled band where the spin-forbidden transition ($^3A_{2g} \rightarrow {}^1E_g$) has a stolen intensity from the spin-allowed one ($^3A_{2g} \rightarrow {}^3T_{1g}$). It is not properly correct to assign one component of the doublet to ^1E_g and the other to $^3T_{1g}$ as they are scrambled by the mechanism of spin−orbit coupling. According to the Tanabe−Sugano diagram, the $^3A_{2g} \rightarrow {}^1E_g$ transition (not allowed according to the selection spin, or Laporte, rule) should appear at 12 600 cm^{-1} ($\mathbf{1_{Ni}}$) and 12 800 cm^{-1} ($\mathbf{2_{Ni}}$). It has to be remarked that the position of ν_2 in $\mathbf{1_{Ni}}$ has been calculated, as a mean value, by the Dou's method. Moreover, on going from $\mathbf{1_{Ni}}$ to $\mathbf{2_{Ni}}$, a shift of the d−d absorption bands (reflected

(15) Tian, Y.-Q.; Cai, C.-X.; Ji, Y.; You, X.-Z. *Angew. Chem., Int. Ed.* **2002**, *41*, 1384; Yang, G. *J. Chem. Crystallogr.* **2004**, *34*, 269.

(16) Lever, A. B. P. *Inorganic Electronic Spectroscopy*; Elsevier: Amsterdam, 1984.

(17) Dou, Y. *J. Chem. Educ.* **1990**, *67*, 134.

Table 1. Summary of Spectroscopic and Magnetic Data for $Co(NP)_2(H_2O)_4$ (**1$_{Co}$**), $Ni(NP)_2(H_2O)_4$ (**1$_{Ni}$**), Crystalline $[Co(NP)_2]_n$ (**3$_{Co}$**), Amorphous $[Ni(NP)_2]_x$ (**2$_{Ni}$**), $[Ni(2\text{-pymo})_2(H_2O)_{2.5}]$, $M(4\text{-pymo})_2(H_2O)_4$, $[M(2\text{-pymo})_2]_n$ (M = Co, Ni), $[Co(4\text{-pymo})_2]_n$, and Amorphous $[Ni(4\text{-pymo})_2]_x$, Electronic Transitions Maxima (ν_i, cm^{-1}), Values of Δ (cm^{-1}), Racah *B* Parameter (cm^{-1}), and *J* (cm^{-1})[a]

Compound	ν_1	ν_2	ν_3	Δ	*B*	*J*	ref
$Co(NP)_2(H_2O)_4$	8850	18920(calc)	21230	10070(Δ_o)	907	n.a.	*b*
$Ni(NP)_2(H_2O)_4$	9480	14970(calc)	23935	9480(Δ_o)	700	n.a.	*b*
$[Co(NP)_2]_n$	5460(calc)	8100	17590	5460(Δ_t)	865	−4.82(2)	*b*
		9360	20000				
		11060					
$[Ni(NP)_2]_x$	8690	14925	22785(calc)	8690(Δ_o)	711	n.a.	*b*
		12980					
$[Ni(2\text{-pymo})_2(H_2O)_{2.5}]_n$	9615	15870	27600	9615(Δ_o)	975	n.a.	*b*
$Co(4\text{-pymo})_2(H_2O)_4$	8680	18530	19960	9840(Δ_o)	830	n.a.	9a
$Ni(4\text{-pymo})_2(H_2O)_4$	9540	15625	25770	9540(Δ_o)	850	−0.313(5)	9b
$[Co(2\text{-pymo})_2]_n$	5500	9345	18480	5500(Δ_t)	755	−3.51(3)	9a
$[Ni(2\text{-pymo})_2]_n$	8810	14815	24570	8810(Δ_o)	864	−7.04(5)	*b*
$[Co(4\text{-pymo})_2]_n$	7935	16965	18975	9025(Δ_o)	810	−1.73(2)	9a
$[Ni(4\text{-pymo})_2]_x$	8770	15340	25380	8770(Δ_o)	960	−4.11(3)	9b

[a] For the calculation of Δ and *B*, see text. The calculated ν_i bands have been estimated with the Dou's method. [b] This work.

by an appreciable color change from blue-green to green) is observed, suggesting a slight change in the coordination environment on passing from **1$_{Ni}$** to **2$_{Ni}$**.

The values of *B*, Δ_o (for **1$_{Co}$**, **1$_{Ni}$**, and **2$_{Ni}$**), and Δ_t (for **3$_{Co}$**) are collected in Table 1. For **1$_{Co}$**, the values of Δ_o and *B* have been calculated by applying the Dou's method. In the case of tetrahedral complexes, the position of the maximum of the first electronic transition, ν_1, coincides with the value of Δ_t. Since ν_1 is undetectable in the spectrum of **3$_{Co}$**, its value has been calculated from those of ν_2 and ν_3 by applying the Dou's method. Regarding ν_2 and ν_3, being multiple bands, an intermediate value of their maxima positions has been taken. In the case of the species of Ni(II), the values of Δ_o and *B* reported here have been obtained, reminding that, for a d^8 electronic configuration, Δ_o coincides with the first electronic transition, ν_1. For comparison, the values for $[Ni(2\text{-pymo})_2(H_2O)_{2.5}]_n$, $M(4\text{-pymo})_2(H_2O)_4$, $[M(2\text{-pymo})_2]_n$ (M = Co, Ni), $[Co(4\text{-pymo})_2]_n$, and amorphous $[Ni(4\text{-pymo})_2]_x$ are reported in Table 1 as well. Notably, despite the different nature of the three ligands, the crystal field splitting of all the species having either an octahedral or a tetrahedral metal center have a comparable energy; thus, it can be reasonably suggested that both a different position of the exocyclic oxygen and the presence of the nitro group do not heavily affect the electronic properties of these systems.

Crystal Structure of $Co(NP)_2(H_2O)_4$ (1$_{Co}$) and $Ni(NP)_2(H_2O)_4$ (1$_{Ni}$). Crystals of $M(NP)_2(H_2O)_4$ (M = Co, **1$_{Co}$** and M = Ni, **1$_{Ni}$**) contain mononuclear *trans*-octahedral $M(1)(N1)_2(O_w)_4$ units (M1, see Figure 3c; N1, coordinated NP nitrogen atom; O_w, coordinated water oxygen atom) in which the metal(II) ions, lying on a crystallographic inversion center (Wyckoff position *a*), are bound to two N1-monodentate NP ligands and to four water molecules (Figure 3a).

It is worth noting that the crystallographically unique M1−N1 bond distance, unconstrained during the final refinement process, reaches a reasonable value [2.192(9) and 2.101(12) Å for **1$_{Co}$** and **1$_{Ni}$**, respectively, consistent with six-coordinated M(II) ions] in agreement with those of the recently reported $M(4\text{-pymo})_2(H_2O)_4$ species[9a,b] [2.159(4) for M = Co and 2.084(3) for M = Ni] and of other octahedral $M(N)_2(H_2O)_4$ fragments retrieved from the CSD. The parallelism between the **1$_M$** species and the $M(4\text{-pymo})_2(H_2O)_4$ analogues can be further drawn, as evidenced in Table 2. Though mononuclear, the latter are interconnected by an extended network of intermolecular hydrogen bonds, so that they could be even described as a supramolecular 3D assembly. Also, in the case of **1$_{Co}$** and **1$_{Ni}$**, a 3D hydrogen-bonded network can be envisaged (Figure 3b), since all four independent water hydrogen atoms are involved in hydrogen bonds with the swinging ends of the NP ligands (namely O1···O3, O1···O32, O2···O3, and O2···N3).

As extensively discussed in the Experimental Section, the XRPD traces suggest the presence of highly defective structures, interpreted in terms of a disordered model "conditioned" within the *ab* plane. Indeed, the metal atoms are partially disordered over two positions, the major one (M1, the only one mentioned above for the sake of clarity) and a minor one, M2, displaced by $(0,{}^1/_2,0)$. This corresponds to a switching of the NP-coordinated nitrogen atom, i.e., $M1(N1)_2(O_w)_4$ vs $M2(N3)_2(O_w)_4$. Basically, as depicted in Figure 3c and d, the $M(NP)_2(H_2O)_4$ unit may be "centered" about two distinct sites, M1 and M2, without a significant change of both its stereochemistry and the overall packing environment, i.e., the $(NP)_2(H_2O)_4$ framework can sustain the metal presence in one site or in the other, provided that the distribution of defects is not random but conditioned. Yet, given the refined occupancy values, the two sites can be considered neither strictly equiprobable nor isoenergetic. The actual position and orientation of both the NP moieties and the water molecules are somewhat influenced by the major metal center, M1. Thus, to adequately describe in detail the coordination sphere of M1, they need to be (only) slightly shifted to account for chemically significant bond values in the case of M2. For example, the present values of the M2−N3 bond, 1.933(9) and 1.946(11) in **1$_{Co}$** and **1$_{Ni}$**, respectively, are likely to be increased up to about 2.1 Å by the correct (re)positioning of the NP. NP aromatic rings stack along **a** with a separation of *a*/2 (3.81 and 3.75 Å for **1$_{Co}$** and **1$_{Ni}$**, respectively).

As shown in Figure 3b, hydrogen-bonded "chains" running along *b*, can be envisaged that are well-separated along *c*. This structural aspect justifies the experimentally observed

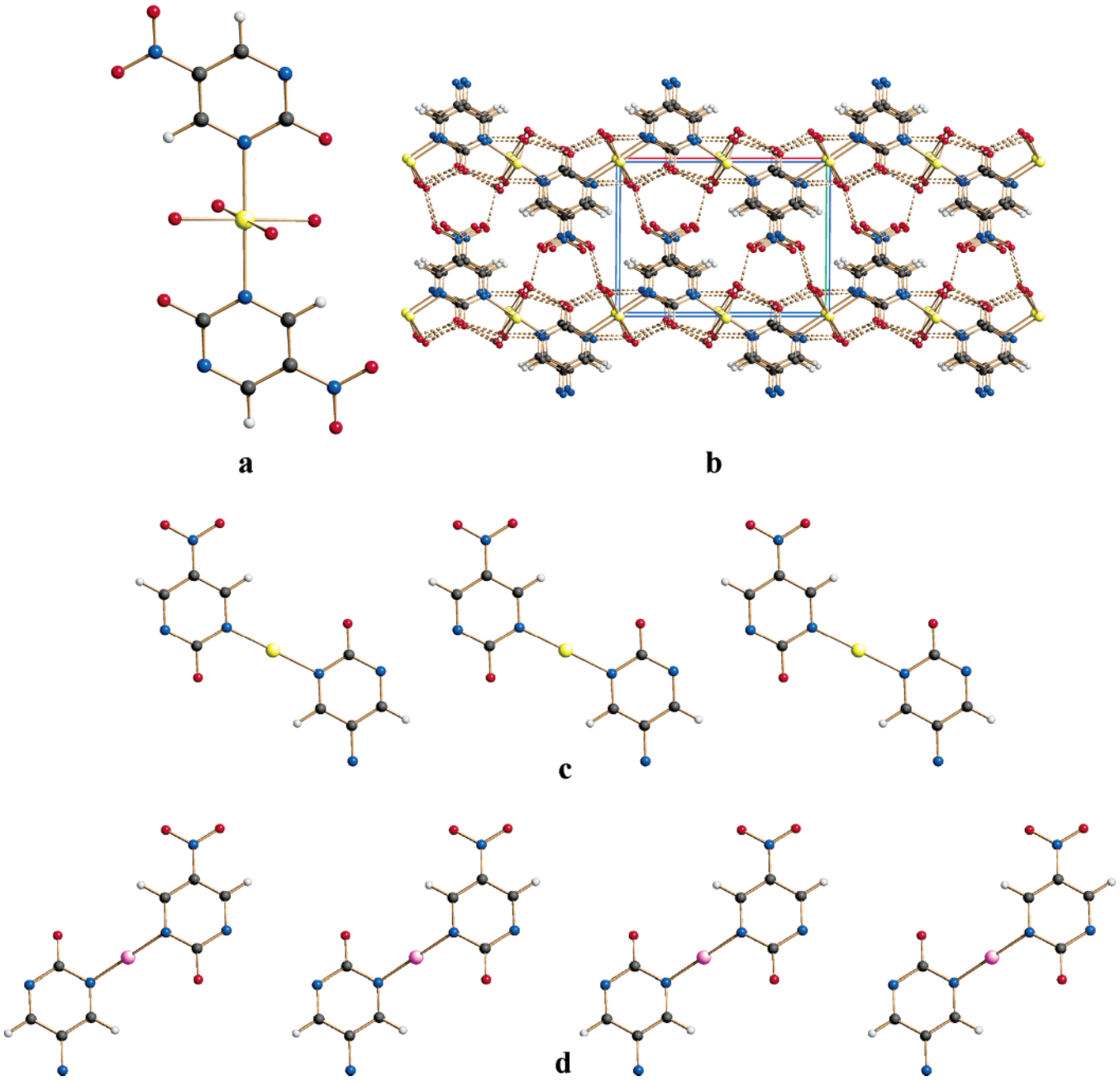

Figure 3. Representation, in $Co(NP)_2(H_2O)_4$ ($\mathbf{1_{Co}}$) of: (a) the metal stereochemistry; (b) the packing motif, viewed down [100]. In (b), the hydrogen−bond interactions have been depicted with dashed lines. (c) Sequence of $\mathbf{1_{Co}}$ along the *a* axis (horizontal; water molecules omitted for clarity), admitting occupancy of the M1 site; at variance, in (d), the M2 site is populated (see text). The metal coordination and the packing motif in $Ni(NP)_2(H_2O)_4$ ($\mathbf{1_{Ni}}$) appears, at the drawing level, identical.

preferred orientation pole [001], which is indicative of easy cleavage along this direction.

Crystal Structure of $[Co(NP)_2]_n$ ($\mathbf{3_{Co}}$) and $[Zn(NP)_2]_n$ ($\mathbf{3_{Zn}}$). The isomorphous species $M(NP)_2$ ($\mathbf{3_{Co}}$ for M = Co and $\mathbf{3_{Zn}}$ for M = Zn) contain one crystallographically independent metal ion, in general position, and two crystallographically independent NP ligands, showing two different coordination modes. One of the NP moieties, lying approximately on the *ac* plane, bridges two metal centers about 5.80 Å away in the common *N*,*N*′-*exo*-bidentate mode. The other ligand, lying approximately on the (201) plane, bridge, in the unusual *N*,*O*-*exo*-bidentate fashion, two metal atoms about 4.82 Å apart. Each metal center thus shows a slightly distorted tetrahedral stereochemistry of MN_3O formulation (Figure 4).

The absence of NP bridging about *a* leads to the formation of 2D slabs running parallel to the *bc* plane. Interactions between successive 2D slabs along *a* (layer separation about 12.5 Å) are hindered by the nitro groups of the NP moieties; actually, the major inertial axis of both the *N*,*N*- and the *N*,*O*-bridging NP moieties lies in the *ac* plane (Figure 5a). Even in this case, the XRPD observation, for both $\mathbf{3_{Co}}$ and $\mathbf{3_{Zn}}$, of a [100] preferred orientation pole thus finds a pertinent structural explanation.

Table 2. Relevant Structural Parameters and Details for $M(XP)_2$ Species

compound[a]	system	SG	*a*, Å	*b*, Å	*c*, Å	*β*, °	structure	M stereoch[b]	M···M, Å	XP coord[c]	rt color	t_{dec} °C	ref
$Co(2P)_2$	tetrag	*I*-42*d*	7.4114(3)	7.4114(3)	17.0879(7)	90	3D	MN_4	5.655	η^1-N, η^1-N′	purple	560	12a
$Co(4P)_2(W)_4$	ortho	*Pcab*	13.5233(4)	12.9617(3)	6.7925(2)	90	0D	MN_2W_4	6.792	η^1-N	pink	150	9a
$Co(4P)_2$	ortho	*Imma*	6.5720(8)	6.6209(8)	20.688(2)	90	2D	$MN_2(N)_2O_2$	6.521, 6.572	η^2-O, (N)-η^1-N′	purple	470	9a
$Co(NP)_2(W)_4$	monocl	$P2_1/a$	7.6207(10)	11.5332(10)	8.6717(5)	101.193(7)	0D	MN_2W_4	5.767[b]	η^1-N	pink	120	this work
$Co(NP)_2$	ortho	*Pcab*	24.8865(19)	9.6718(7)	9.4462(6)	90	2D	MN_3O	4.837, 5.798	η^1-N-η1-N′ η^1-N′ η^1-O	purple	460	this work
$Ni(2P)_2(W)_{2.5}$	tetrag	$P4_2/nmc$	12.6531(4)	12.6531(4)	14.5844(9)	90	2D	MN_4W_2	6.327	η^1-N-η^1-N′	green	200	12a
$Ni(2P)_2$	ortho	*Fdd*2	11.0361(8)	9.6611(8)	16.1935(8)	90	3D	MN_4O_2	5.462	η^2-N, O-η^1-N′	green	550	12a
$Ni(4P)_2(W)_4$	ortho	*Pcab*	13.4276(4)	12.9033(5)	6.7550(2)	90	0D	MN_2W_4	6.754	η^1-N	blue-green	140	9b
$Ni(4P)_2$	tetrag	*I*-4/*amd*	6.5141(7)	6.5141(7)	20.931(3)	90	2D	$MN_2(N)_2O_2$	6.514	η^2-O, (N)-η^1-N′	green	388	9b
$Ni(NP)_2(W)_4$	monocl	$P2_1/a$	7.5030(7)	11.4658(8)	8.7506(5)	101.781(8)	0D	MN_2W_4	5.733[b]	η^1-N	green	180	this work
$Zn(2P)_2$	tetrag	*I*-42*d*	7.3919(2)	7.3919(2)	17.3389(6)	90	3D	MN_4	5.696	η^1-N-η^1-N′	white	570	12a
$Zn(4P)_2$	trig	*R*3*c*	21.0415(4)	21.0415(4)	11.4294(2)	90	3D	MN_3O	5.72, 7.05	η^1-N-η^1-N′ η^1-N, η^1-O	white	285	9b
$Zn(NP)_2$	ortho	*Pcab*	25.3228(8)	9.6270(3)	9.4320(3)	90	2D	MN_3O	4.813, 5.810	η^1-N-η^1-N′ η^1-N, η^1-O	white	490	this work

[a] 2P: 2-pyrimidinolate; 4P: 4-pyrimidinolate; NP: 5-nitro-2-pyrimidinolate; W: water molecule. [b] W: water oxygen. [c] In parentheses, long-range, nonbonding interactions are reported.

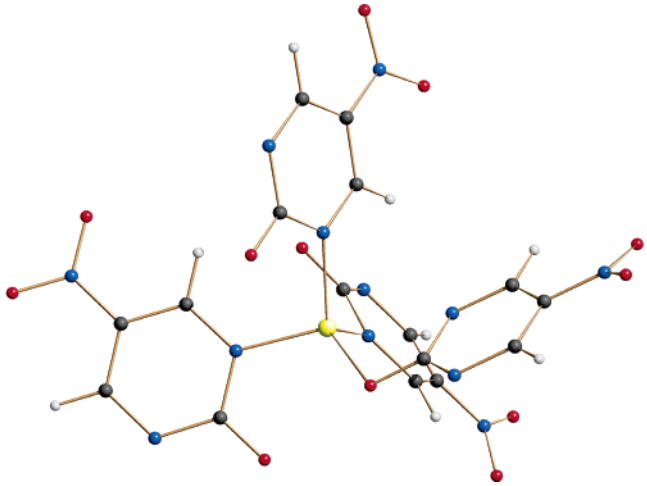

Figure 4. Representation of the stereochemistry at the metal in $[M(NP)_2]_n$, (M = Co and Zn).

Focusing the attention just on the skeleton of the slabs formed by the NP bridged metal centers, a 2D wavy structural motif can be easily envisaged, composed of rectangular meshes having the NP ligands as edges and the metals as vertexes (Figure 5b). Topologically speaking, this 2D array was already observed in $[M(4\text{-pymo})_2]_n$ (M = Co[9a] and Ni[9b]), although in the latter the metals were strictly coplanar and a single type of ligand coordination was observed.

Metal centers having the MN_3O chromophore, as in $\mathbf{3_M}$, were previously found in the $[Zn(4\text{-pymo})_2]_n$ species, where the two crystallographically independent 4-pymo moieties act in the *N*,*N*′- and *N*,*O*-*exo*-bidentate fashions, generating an unprecedented 3D interpenetrated network.[9b] At variance, 2-pymo always prefers the usual *N*,*N*′-*exo*-bidentate coordination mode, as occurs in the 3D diamondoid network of the isomorphous species $[M(2\text{-pymo})_2]_n$ (M = Co and Zn).[12a]

The examples presented above (and collectively reported in Table 2) introduce other considerations involving the kind of atoms bound to the metal when pyrimidinolate ligands are involved: (i) hydrated zinc species have never been obtained, either by varying the position of the exocyclic oxygen or the substitution on the pyrimidinic ring; indeed, this metal center invariably prefers tetrahedral (rather than octahedral) stereochemistry, thus impeding further ligand coordination by, for example, water molecules; (ii) both zinc and cobalt have already shown a certain propensity to coordinate the pymo oxygen: valuable examples are the homoleptic compounds $[M(4\text{-pymo})_2]_n$, showing rather different structures (2D-layered in the case of Co,[9a] 3D-diamondoid interpenetrated for Zn[9b]) and the isomorphous, mixed-ligand species $M(2\text{-pymo})_2(N_2H_4)_2$ (M = Co, Ni, and Zn),[12a] where 2-pymo acts in the uncommon monodentate O-coordination mode.

Magnetic Properties of $Co(NP)_2(H_2O)_4$ ($\mathbf{1_{Co}}$), $Ni(NP)_2(H_2O)_4$ ($\mathbf{1_{Ni}}$), $[Ni(NP)_2]_x$ ($\mathbf{2_{Ni}}$), and $[Co(NP)_2]_n$ ($\mathbf{3_{Co}}$). For both $\mathbf{1_{Co}}$ and $\mathbf{1_{Ni}}$, we performed room-temperature measurements of the magnetic behavior calculating the effective magnetic moment (μ_{eff} respective values of 4.62 and 3.09 μ_B). If compared with the theoretical values calculated for $g = 2$, the μ_{eff} found for $\mathbf{1_{Ni}}$ is typical of an isolated metal center with two unpaired electrons; in the case of $\mathbf{1_{Co}}$, a value higher than that expected for three unpaired electrons has been obtained because of the presence of the spin−orbit coupling typical of a $^4T_{1g}$ state.

For $\mathbf{3_{Co}}$ and $\mathbf{2_{Ni}}$, variable temperature measurements of χ_M, in the 2−300 K and 80−290 K range, respectively, have been performed (Figure 6). In the case of $\mathbf{3_{Co}}$, as shown in Figure 6, χ_M increases upon cooling until 23 K in which a maximum is reached. The $\chi_M T$ values steadily decrease on lowering the temperature. Taking into account the $^4A_2$ electronic ground state for $\mathbf{3_{Co}}$ (see Figure 6), the thermal behavior of the magnetic measurements is typical of an antiferromagnetic behavior taking place between the metal centers, which is transmitted through the NP bridges. In the case of $\mathbf{2_{Ni}}$, the $\chi_M T$ values are almost constant in the temperature range studied, which is indicative of small magnetic interactions taking place in this material.

The magnetic behavior of $\mathbf{3_{Co}}$ can be reasonably interpreted through eq 1, describing the high temperature dependence

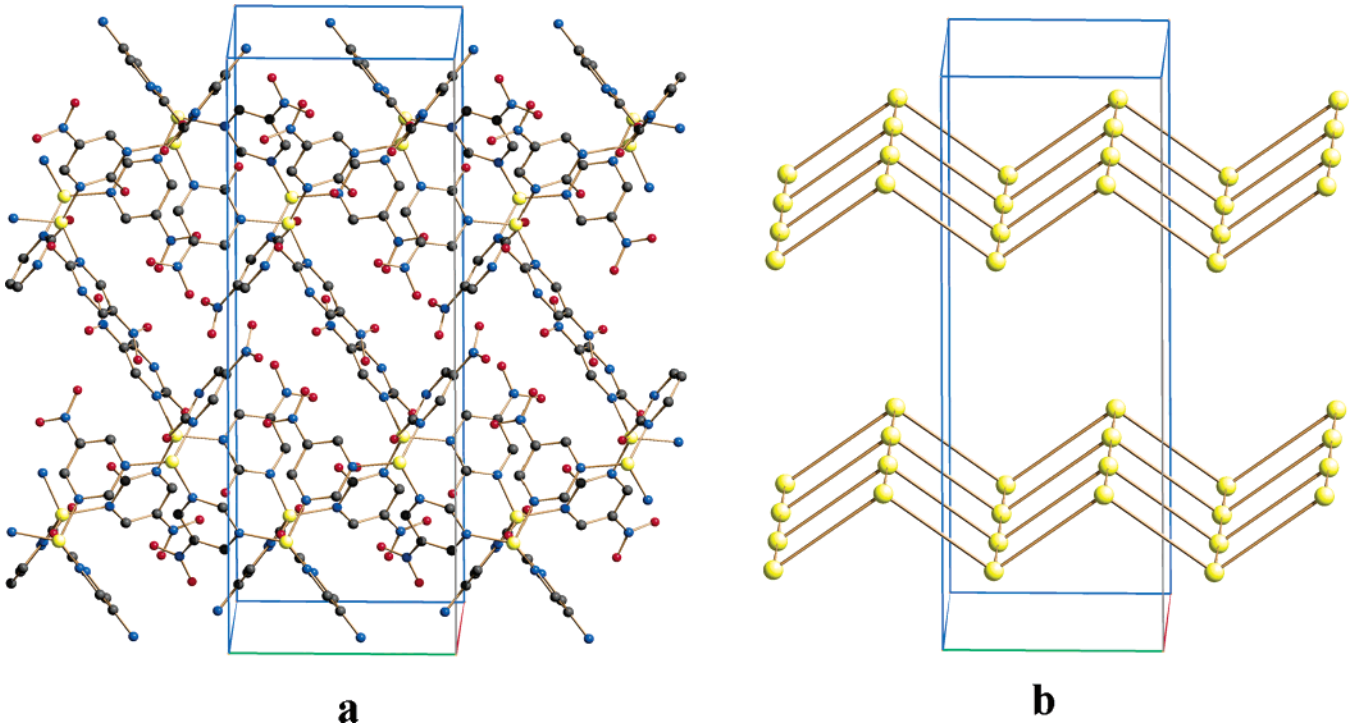

Figure 5. Representation, in $[Zn(NP)_2]_n$ ($\mathbf{3_{Zn}}$) of: (a) the packing motif viewed approximately down [010]; (b) the wavy motif described by the metal skeleton, viewed approximately down [010]. In (b), just NP-bridged metal atoms are depicted for clarity. In both cases, the structure of $[Co(NP)_2]_n$ ($\mathbf{3_{Co}}$) is, at the drawing level, identical.

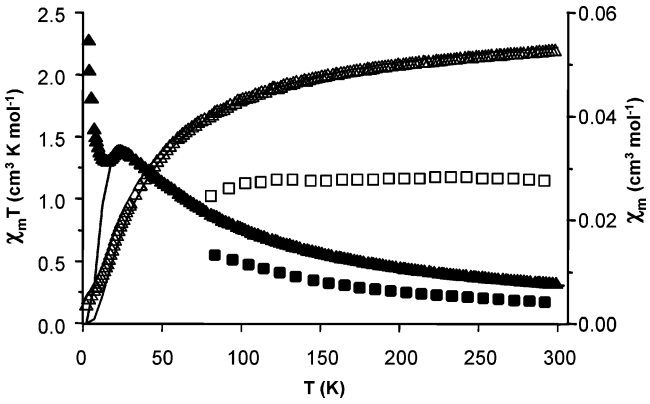

Figure 6. χ_M and $\chi_M T$ values for $[Co(NP)_2]_n$ (▲ and △, respectively) and $[Ni(NP)_2]_x$ (■ and □, respectively) in the 2−300 and 80−290 K temperature range at a field strength of 10 and 18 kG, respectively. The solid lines represent the fitting obtained with eq 1.

of $\chi_M T$ on a 2D Heisenberg quadratic-layer antiferromagnet:

$$\chi T = \frac{N g^2 \mu_B{}^2 T}{J\left(3\theta + \sum_{n=1}^{\infty} \frac{C_n}{\theta^{n-1}}\right)} \qquad (1)$$

where the spin Hamiltonian is defined as $H = \sum J S_i S_j$,[18] $\theta = kT/JS(S+1)$, g is the Landè factor, μ_B is the Bohr magneton, N is the number of spins in the lattice, and the C_n coefficients have been taken from ref 18b. Fitting the data to eq 1, g and J exchange values of 2.30(1) and −4.82(2) cm^{-1} have been obtained. The J exchange value found for $\mathbf{3_{Co}}$ is comparable to that obtained for the related $[Co(2\text{-pymo})_2]_n$ system [−3.51(3) cm^{-1}] with the 2-pymo also exhibiting a *N*,*N*′-*exo*-bidentate coordination mode but larger than that for the $[Co(4\text{-pymo})_2]_n$ system [−1.73(2) cm^{-1}] in which 4-pymo exhibits a *N*,*O*′-*exo*-bidentate coordination mode with additional long-range Co···N interactions.[9a] It should be noted that, in contrast to the $[Co(2\text{-pymo})_2]_n$ system, for both $[Co(NP)_2]_n$ and $[Co(4\text{-pymo})_2]_n$ no spin canting is observed, which may be attributed to the centrosymmetric nature of the latter.

(18) (a) Lines, M. E. *J. Phys. Chem. Solids* **1970**, *31*, 101. (b) Rushbrooke, G. S.; Wood, P. J. *Mol. Phys.* **1958**, *1*, 257.

Conclusions

The HNP species, in its deprotonated form, has been used for the first time in building coordination complexes. Typically, the NP moiety has been found to coordinate through (at least) one nitrogen atom, assisted by *N*- or even *O*-coordination, in the *N*,*N*′- or *N*,*O*′-*exo*-bidentate fashions, respectively. The latter, although not unexpected, was not observed in the corresponding unsubstituted M(II) pyrimidin-2-olates, where the metals were bridged by *N*,*N*′-ligands and kept ∼5.8 Å apart. In all the presented species, the nitro group is not involved in metal coordination, in agreement with its low Lewis basicity.

Once again, we show the suitability of the XRPD methods for the ab initio structural characterization of polycrystalline coordination compounds as well as their corresponding solid-to-solid reaction products. Indeed, the here reported materials are ideally suited for this methodology, owing to the impossibility of obtaining them as single crystals and to the reversible polymerization reactions taking place upon dehydration/rehydration processes.

Unfortunately, within the group of structures reported above, none crystallized in an acentric space group, thus partially diminishing our efforts in finding potentially SHG-active $M(NP)_2$ species for which an extremely high hyperpolarizability is expected.[19] Possibly, the use of different metals and, eventually, of ancillary ligands may result in discovering new crystal architectures suitable for solid-state SHG. Work can be anticipated in the direction of synthesis and complete characterization of noncentrosymmetric M(NP) species with metals in +I oxidation state, such as Cu(I)[20] and Ag(I) ions. Indeed, these metals, when linearly coordinated, have been shown to afford helical polymeric systems similar to polymetaaryls.[21] Even if noncentrosymmetric crystals are not granted by this fact alone, this structural motif can indeed represent a prerequisite for SHG activity.

Experimental Section

General Methods. 5-Nitro-pyrimidine-2-ol (NP) was prepared according to literature methods.[13] Microanalyses of C, H, and N were performed with a Fisons-Instruments EA-1008 analyzer. Thermogravimetric and differential scanning calorimetric analyses were performed, under a reactive atmosphere of air, on Shimadzu-TGA-50H/DSC equipment at heating rates of 20 °C min^{-1} and 10 °C min^{-1}, respectively (Scientific Instrumentation Center of the University of Granada). Magnetic susceptibility measurements were performed on polycrystalline samples with a quantum design MPMS-2 SQUID magnetometer (Complutense University) operating at 10 kG in the temperature range 2.0−300 K ($\mathbf{3_{Co}}$), whereas compounds $\mathbf{1_{Co}}$, $\mathbf{1_{Ni}}$, and $\mathbf{2_{Ni}}$ were measured on Manics DSM-8 equipment. The first two species were measured at room temperature, whereas the $\mathbf{2_{Ni}}$ was only measured in the 80−290 K temperature range. Electronic spectra on polycrystalline samples were carried out on a Varian Cary UV−vis−NIR spectrophotometer in the reflectance mode (Scientific Instrumentation Center of the University of Granada). IR spectra were recorded in the 4000−300 cm^{-1} range on a Midac FT-IR using KBr pellets.

Preparation of $M(NP)_2(H_2O)_4$ ($\mathbf{1_M}$) (M = Co, Ni). A colorless aqueous solution of $HNP{\cdot}H_2SO_4$ (1.5 mmol in 20 mL) with an initial pH = 1 was treated with NEt_3 until the pH rose to 6.5 and a concomitant yellow dyeing of the solution was observed. Afterward, an aqueous solution of $M(ClO_4)_2{\cdot}6H_2O$ (0.75 mmol in 10 mL) was added. **Caution!** Perchlorate salts are potentially explosive and should be used in small quantities. After a few hours, a pale-green microcrystalline precipitate corresponding to $\mathbf{1_{Ni}}$ appeared, while a pink microcrystalline precipitate of $\mathbf{1_{Co}}$ formed within 1 day. $\mathbf{1_{Ni}}$: Yield 40−50%. Anal. Calcd for $C_8H_{12}N_6O_{10}Ni$: C, 23.41; H, 2.93; N, 20.49. Found: C, 23.30; H, 2.64; N, 20.31. IR (selected bands in cm^{-1}): 3490 vs; 1604 vs, 1560 vs, 1336 vs, 1285 s, 1162 m, 1137 m, 817 s, 688 s, 509 m. $\mathbf{1_{Co}}$: Anal. Calcd for $C_8H_{10}N_6O_9Co$: C, 24.55; H, 2.56; N, 21.48. Found: C, 24.55; H, 2.60; N, 21.42. IR (selected bands in cm^{-1}): 3490 vs, 1610 vs, 1563 vs, 1342 vs, 1285 s, 1163 m, 1137 m, 817 s, 688 s, 516 m.

Preparation of $[Co(NP)_2]_n$ ($\mathbf{3_{Co}}$). $\mathbf{3_{Co}}$ can be prepared either using a direct synthetic method or by thermal treatment of $\mathbf{1_{Co}}$.

Direct Synthetic Method. An ethanolic solution containing $HNP{\cdot}H_2SO_4$ (1.5 mmol) and NEt_3 (3 mmol) in 20 mL was mixed with another one containing $Co(ClO_4)_2{\cdot}6H_2O$ (0.75 mmol in 10 mL); a purple powder immediately precipitated. Yield 50%. Anal. Calcd for $C_8H_4N_6O_6Co$: C, 28.34; H, 1.19; N, 24.78. Found: C, 28.10; H, 1.25; N, 24.62. IR (selected bands in cm^{-1}): 3425 m, 1664 vs, 1604 vs, 1580 vs, 1328 vs, 1280 s, 1156 m, 814 s.

Thermal Treatment of $\mathbf{1_{Co}}$. Compound $\mathbf{1_{Co}}$ (25 mg) was heated under dinitrogen at 140° C for 20 min. In this way, the purple amorphous $\mathbf{2_{Co}}$ phase was obtained. The progressive cooling of the sample within 30 min yielded crystalline $\mathbf{3_{Co}}$. Yield 100%. Anal. Calcd for $C_8H_4N_6O_6Co$: C, 28.34; H, 1.19; N, 24.78. Found: C, 28.13; H, 1.24; N, 24.67. IR (selected bands in cm^{-1}): 3425 m, 1664 vs, 1604vs, 1580 vs, 1328 vs, 1280 s, 1156 m, 814 s.

Preparation of $[Ni(NP)_2]_x$ ($\mathbf{2_{Ni}}$). As well as for $\mathbf{2_{Co}}$, we attempted the synthesis of $\mathbf{3_{Ni}}$ by both a direct synthetic procedure and thermal treatment of $\mathbf{1_{Ni}}$. In this case, we succeeded in isolating $\mathbf{2_{Ni}}$ only by the latter route.

Thermal Treatment of $\mathbf{1_{Ni}}$. Compound $\mathbf{1_{Ni}}$ (25 mg) was heated under dinitrogen at 150 °C for 20 min giving a green powder analyzing as $\mathbf{2_{Ni}}$. Yield 100%. Anal. Calcd for $C_8H_4N_6O_6Ni$: C, 28.36; H, 1.19; N, 24.80. Found: C, 28.20; H, 1.12; N, 24.70. IR (selected bands in cm^{-1}): 3390 m, 1597 vs, 1331 vs, 1272 s, 1162 m, 815 s, 691 s.

Preparation of $[Zn(NP)_2]_n$ ($\mathbf{3_{Zn}}$). Using the same procedure for the synthesis of $\mathbf{1_M}$, a white microcrystalline powder corresponding to $\mathbf{3_{Zn}}$ precipitated in a few minutes. $\mathbf{3_{Zn}}$: Yield 50%. Anal. Calcd for $C_8H_4N_6O_6Zn$: C, 27.82; H, 1.15; N, 24.35. Found: C, 27.69; H, 0.83; N, 24.05. IR (selected bands in cm^{-1}): 1654 s, 1611 s, 1580 s, 1330 vs, 1278 m, 1175 m, 1155 m, 817 s, 805 s, 701 m.

X-ray Powder Diffraction Analysis of $Co(NP)_2(H_2O)_4$ ($\mathbf{1_{Co}}$), $Ni(NP)_2(H_2O)_4$ ($\mathbf{1_{Ni}}$), $[Co(NP)_2]_n$ ($\mathbf{3_{Co}}$), and $[Zn(NP)_2]_n$ ($\mathbf{3_{Zn}}$). The powders were gently ground in an agate mortar and then deposited with care in the hollow of an aluminum holder equipped with a zero background plate (supplied by The Gem Dugout, State College, PA). Diffraction data (Cu Kα, $\lambda = 1.5418$ Å) were collected on a θ:θ Bruker Axs D8 Advance ($\mathbf{3_{Co}}$ and $\mathbf{3_{Zn}}$) or on a θ:2θ Philips PW1820 ($\mathbf{1_{Co}}$ and $\mathbf{1_{Ni}}$) vertical scan diffractometer, both equipped with primary and secondary Soller slits, a secondary beam curved graphite monochromator, a Na(Tl)I scintillation detector, and pulse height amplifier discriminator. Generators were operated at 40 kV and 40 mA. Optics used D8/Philips: divergence 0.5/1.0°, antiscatter 0.5/1.0°, receiving 0.2/0.2 mm. Nominal resolutions of the present set-ups are 0.07 and 0.12° 2θ, on D8 and Philips, respectively, for the Si(111) peak at 28.44° (2θ, α_1 component). Long scans were performed with $5 < 2\theta < 105°$ with $t = 30$ s and $\Delta 2\theta = 0.02°$.

While for $\mathbf{3_{Zn}}$ indexing was obtained with the aid of TREOR[22] [orthorhombic, $a = 25.38$ Å, $b = 9.65$ Å, $c = 9.45$ Å, $M(20)$[23] = 15, $F(20)$[24] = 30(0.009, 72)], in the case of $\mathbf{1_{Co}}$, the single value decomposition approach,[25] as implemented in the Topas-R suite of programs,[26] was applied [monoclinic, $a = 7.65$ Å, $b = 11.55$ Å, $c = 8.68$ Å, $\beta = 101.0°$, $M(16)$[23] = 22]. Systematic absences indicated *Pcab* and $P2_1/a$ as the probable space groups, later confirmed by successful solution and refinement. Visual inspection suggested the strict isomorphous character of $\mathbf{1_{Ni}}$ with $\mathbf{1_{Co}}$ and that of $\mathbf{3_{Co}}$ with $\mathbf{3_{Zn}}$. For $\mathbf{1_{Co}}$ and $\mathbf{3_{Zn}}$, structure solutions were performed

(19) The NP ligand belongs both to the class of highly dipolar nitroaromatics and to that of substituted cyclic ureas (uracyls), which are among the most effective organic NLO chromophores. See Nicoud, J. F.; Twieg, R. J. In *Nonlinear Optical Properties of Organic Molecules in Crystals*; Chemla, D. S., Zyss, J., Eds.; Academic Press: Orlando, FL, 1987; Vol. 1.
(20) Masciocchi, N.; Ardizzoia, G. A.; LaMonica, G.; Maspero, A.; Sironi, A. *Angew. Chem., Int. Ed.* **1998**, *37*, 3366.
(21) Rowan, A. E.; Nolte, R. J. M. *Angew. Chem., Int. Ed.* **1998**, *37*, 63.
(22) Werner, P. E.; Eriksson, L.; Westdahl, M. *J. Appl. Crystallogr.* **1985**, *18*, 367.
(23) De Wolff, P. M. *J. Appl. Crystallogr.* **1968**, *1*, 108.
(24) Smith, G. S.; Snyder, R. L. *J. Appl. Crystallogr.* **1979**, *12*, 60.
(25) Coelho, A. A. *J. Appl. Crystallogr.* **2003**, *36*, 86.
(26) Bruker AXS 2003, Topas-R: General profile and structure analysis software for powder diffraction data.

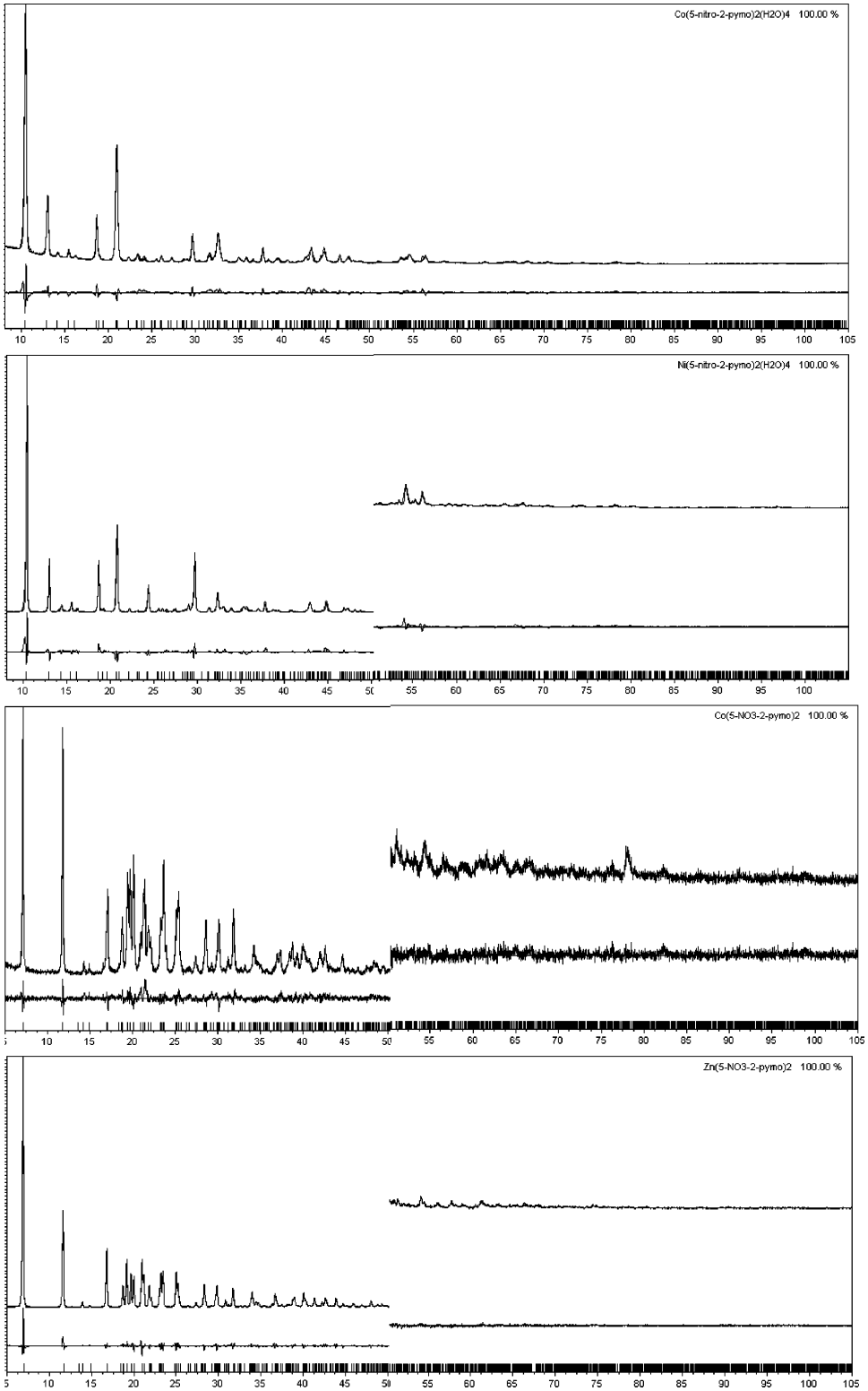

Figure 7. From top, Rietveld refinement results for $Co(NP)_2(H_2O)_4$ (**1_{Co}**), $Ni(NP)_2(H_2O)_4$ (**1_{Ni}**), $[Co(NP)_2]_n$ (**3_{Co}**), and $[Zn(NP)_2]_n$ (**3_{Zn}**), as appreciable from experimental, calculated, and difference diffraction patterns. Peak markers at the bottom. For the sake of clarity, in some cases, the portion above 50° has been magnified (5×). Horizontal axis: 2θ, deg. Vertical axis: counts au.

by using the simulated annealing[27] technique implemented in TOPAS. 5-Nitro-2-pymo ligands were treated as rigid bodies (flexible at the $C-NO_2$ torsion), assigning average literature bond distances and angles (for the heteroaromatic ring: C−C and C−N = 1.40 Å; C−O = 1.25 Å; C−H = 0.95 Å; ring bond angles = 120.0°; for the nitro group: C−N 1.25 = Å, N−O = 1.40 Å; N−O−N = 120.0°, C−N−O = 120.0°). The final refinements were performed by the Rietveld method using TOPAS, maintaining the rigid bodies described above. Peak shapes were described by the fundamental parameters approach.[28] The experimental background

(27) Coelho, A. A. *J. Appl. Crystallogr.* **2000**, *33*, 899.

(28) Cheary, R. W.; Coelho, A. A. *J. Appl. Crystallogr.* **1992**, *25*, 109.

Table 3. Crystal Data and Refinement Details for Compounds $Co(NP)_2(H_2O)_4$ (**1$_{Co}$**), $Ni(NP)_2(H_2O)_4$ (**1$_{Ni}$**), $[Co(NP)_2]_n$ (**3$_{Co}$**), and $[Zn(NP)_2]_n$ (**3$_{Zn}$**)

compound	$Co(NP)_2(H_2O)_4$	$Ni(NP)_2(H_2O)_4$	$Co(NP)_2$	$Zn(NP)_2$
indexing method	SVD[25]	n.a.	n.a.	TREOR90[22]
indexing FoM	$M(16) = 22$[23]	n.a.	n.a.	$M(20) = 15$[23]
				$F(20) = 30(0.009, 72)$[24]
system	monoclinic	monoclinic	orthorhombic	orthorhombic
SPGR	$P2_1/a$	$P2_1/a$	*Pcab*	*Pcab*
a, Å	7.6207(10)	7.5030(7)	24.8865(19)	25.3228(8)
b, Å	11.5332(10)	11.4658(8)	9.6718(7)	9.6270(3)
c, Å	8.6717(5)	8.7506(5)	9.4462(6)	9.4320(3)
α, deg	90	90	90	90
β, deg	101.193(7)	101.781(8)	90	90
γ, deg	90	90	90	90
V, Å^3	747.3(1)	736.9(1)	2273.7(3)	2299.3(1)
Z	2	2	8	8
fw, g mol^{-1}	411.15	410.9	339.1	345.6
ρ_{calc}, g cm^{-3}	1.826	1.852	1.981	1.996
F(000)	418	420	1352	1376
μ(Cu Kα), cm^{-1}	96.8	26.0	123.1	34.3
diffractometer	Philips PW1820	Philips PW1820	Bruker D8	Bruker D8
T, K	298(2)	298(2)	298(2)	298(2)
2θ range, deg	5−105	5−105	5−105	5−105
N_{data}	5001	5001	5001	5001
N_{obs}	858	845	1303	1318
R_p, R_{wp}[a]	0.076, 0.101	0.121, 0.166	0.097, 0.126	0.098, 0.128
R_{Bragg}[a]	4.17	8.86	3.65	3.45
χ^2[a]	4.01	7.86	1.26	1.98
V/*Z*, Å^3	186.7	184.2	284.2	287.4
pref orient pole	0 0 1	0 0 1	1 0 0	1 0 0

[a] $R_p = \sum_i |y_{i,o} - y_{i,c}|/\sum_i |y_{i,o}|$; $R_{wp} = [\sum_i w_i (y_{i,o} - y_{i,c})^2/\sum_i w_i (y_{i,o})^2]^{1/2}$; $R_B = \sum_n |I_{n,o} - I_{n,c}|/\sum_n I_{n,o}$; $\chi^2 = \sum_i w_i (y_{i,o} - y_{i,c})^2/(N_{obs} - N_{par})$, where $y_{i,o}$ and $y_{i,c}$ are the observed and calculated profile intensities, respectively, while $|F_{n,o}|$ and $|F_{n,c}|$ are the observed and calculated integrated intensities. The summations run over *i* data points or *n* independent reflections. Statistical weights w_i are normally taken as $1/y_{i,o}$.

was fit by a polynomial description. Systematic errors were modeled with sample-displacement angular shifts, preferred orientation corrections in the March−Dollase[29] formulation (with [001], [001], [100], and [100] poles in **1$_{Co}$**, **1$_{Ni}$**, **3$_{Co}$**, and **3$_{Zn}$**, respectively) and anisotropic peak shape broadening (**1$_{Co}$**, **1$_{Ni}$**, and **3$_{Co}$**).[28] Metal atoms were given a refinable isotropic displacement parameter (B_M), while lighter atoms were assigned a common $B = B_M + 2.0$ Å^2 value. Scattering factors, corrected for real and imaginary anomalous dispersion terms, were taken from the internal library of TOPAS.

Regarding compounds **1$_{Co}$** and **1$_{Ni}$**, some features present in their XRPD traces, such as anisotropic peak broadening and peak tails, remained unexplained at the end of Rietveld refinements practically driven to convergence. This suggested the presence of a defective structure, described introducing a "conditionally" disordered model. The latter was completed by calculating a difference Fourier map at the end of a Rietveld refinement carried out with the ordered model: a non negligible peak was clearly present in the *c* Wyckoff position, this site being proper to host the metal ion (site occupancies of about 0.19 and 0.35 were found for **1$_{Co}$** and **1$_{Ni}$**, respectively).

Final R_p, R_{wp}, R_{Bragg} and χ^2 agreement factors, details on data collections and analyses for **1$_{Co}$**, **1$_{Ni}$**, **3$_{Co}$**, and **3$_{Zn}$** can be found in Table 3. Figure 7 shows the final Rietveld refinement plots.

Crystallographic data (excluding structure factors) for the structures reported in this paper have been deposited with the Cambridge Crystallographic Data Centre as supplementary publication Nos. CCDC 252050, 252051, 252052, and 252053. Copies of the data can be obtained free of charge on application to CCDC, 12 Union Road, Cambridge CB2 1EZ, UK (fax: (+44)1223 336−033; e-mail: deposit@ccdc.cam.ac.uk).

Acknowledgment. The Italian Ministry for Education and Research (MIUR - Azione Integrata Italia-Spagna), the University of Insubria (Progetto di Ateneo "Sistemi Poliazotati"), and the Fondazione Provinciale Comasca are acknowledged for funding. We also thank the Spanish Ministry of Science and Technology through Project BQU2001-2955-CO2-01 and the "Acción Integrada Hispano-Italiana" HI2003-0081. E.B. thanks the Spanish Ministry of Education and Science for a FPU fellowship.

Supporting Information Available: Crystallographic data for compounds **1$_{Co}$**, **1$_{Ni}$**, **3$_{Co}$**, and **3$_{Zn}$** in CIF format. This material is available free of charge via the Internet at http://pubs.acs.org.

IC048539B

(29) (a) March, A. *Z. Kristallogr.* **1932**, *81*, 285. (b) Dollase, W. A. *J. Appl. Crystallogr.* **1987**, *19*, 267.